Chapter 4

Refractivity measurement

The most abundant gaseous products of an SF_6 discharge are SOF_2 and SO_2 (Mortensen *et al.*, 1994; Belmadani *et al.*, 1991A). Their sum ($SOF_2 + SO_2$) increases during a discharge and their ratio depends on the initial water content within the discharge chamber or switchgear device (Belmadani *et al.*, 1991A). SO_2 is produced by the reaction

$$SOF_2 + H_2O \rightarrow SO_2 + 2HF \qquad (4.1)$$

Both gases (SOF_2 and SO_2) have an index of refraction lower then SF_6: 1.00062166 for SOF_2 (this work, 101325 Pa, T=25 °C, 632.99 nm) and 1.000686 (Gray, 1972) for SO_2, (101325 Pa, 0 °C, 589.6 nm) while SF_6 has a value of 1.00070296 (this work, 101325 Pa, T=25 °C, 632.99 nm). This means that the refractive index of the gas mixture in the discharge chamber, measured at 101325 Pa and 25 °C, decreases with discharge time. As SF_6 molecules are dissociated during a discharge and other molecules produced, the pressure in the chamber rises. The refractive index of the resultant gas mixture at that high pressure is higher, but the index of refraction of the same gas mixture measured at normal conditions (101325 Pa and 25 °C) decreases, because the concentration of SF_6 decreases. All other gases produced in the discharge chamber have lower indices of refraction then SF_6 except SOF_4 and SO_2F_2. There are no data available for these gases but it can be estimated (see Appendix 1) that their refractive indices are 1.000818 and 1.000877, respectively. However, the concentrations of these gases produced in the discharge are much smaller than those of SO_2 and SOF_2. Because SOF_2 is an important product of the SF_6 discharge, and therefore is a significant contributor to the mean refractive index of the SF_6 discharge gas mixture, and because no data on its

refractive index are available in the literature, a measurement was made of the refractive index of SOF_2.

4.1. Measurement of the refractive indices of SOF_2 and SF_6

4.1.1. The non-linearity of the refractive index of gases

The relation between refractive index n and gas density ρ is given by the Lorentz - Lorenz formula (St-Arnaud and Bose, 1979)

$$\frac{n^2-1}{n^2+2} = A_R \rho + B_R(T) \rho^2 \tag{4.2}$$

where A_R and $B_R(T)$ are the first and second refractive virial coefficients, respectively. A_R depends only on wavelength, while $B_R(T)$ is a function of both wavelength and temperature. Both parameters are determined experimentally. The density ρ, is given by the virial equation of state (Thomas and Tayag, 1988):

$$\frac{p}{RT} = \rho + B_p(T) \rho^2 + \ldots \tag{4.3}$$

where $B_p(T)$ is the second virial coefficient of state. The refractivity $(n - 1)$ can be written in the form:

$$n - 1 = A \frac{p}{RT} + B(T) \left(\frac{p}{RT}\right)^2 \tag{4.4}$$

In order to find the relations between the coefficients A and $B(T)$ and the coefficients A_R and $B_R(T)$, the function

$$\frac{n^2-1}{n^2+2} \tag{4.5}$$

is developed into a Taylor series around $n = 1$. This gives:

$$A_R \rho + B_R(T) \rho^2 = \frac{n^2 - 1}{n^2 + 2} \approx \frac{2}{3}(n-1) - \frac{1}{9}(n-1)^2 - \frac{4}{27}(n-1)^3 + \ldots \quad (4.6)$$

When p/RT from equation 4.3 is substituted in equation 4.4, we obtain:

$$n - 1 = A\rho + (AB_p + B)\rho^2 + \ldots \quad (4.7)$$

Substitution of $(n\text{-}1)$ from equation 4.7 into equation 4.6, yields

$$A_R \rho + B_R(T) \rho^2 + \ldots \approx \frac{2}{3}(A\rho + AB_p \rho^2 + B\rho^2) - \frac{1}{9}(A\rho + AB_p\rho^2 + B\rho^2)^2 + \ldots \quad (4.8)$$

or

$$A_R \rho + B_R(T) \rho^2 + \ldots \approx \frac{2}{3} A\rho + \left(\frac{2}{3} AB_p + \frac{2}{3} B - \frac{1}{9} A\right)\rho^2 + \ldots \quad (4.9)$$

Equation 4.9 reveals that the coefficients A and $B(T)$ are related to the coefficients A_R and B_R by

$$A_R = \frac{2}{3} A \quad (4.10)$$

and

$$B_R(T) = \frac{2}{3} B(T) + \frac{2}{3} A B_p(T) - \frac{1}{9} A^2 . \quad (4.11)$$

In equations 4.2, 4.3 and 4.4, the higher order terms are neglected because their influence only becomes important for SF_6 and SOF_2 pressures above 10 atm; and in this work pressures were always below 1.1 atm.

4.1.2. Experimental arrangement

The experimental arrangement is depicted in Figures 4.1 and 4.2. A Lee-Woolsey polarisation interferometer (Lee and Woolsey, 1981) was used to make the measurements of refractive index. This interferometer uses only prisms and is up to 20 times less sensitive to external vibrations than more conventional mirror interferometers (Woolsey *et al.*, 1986).

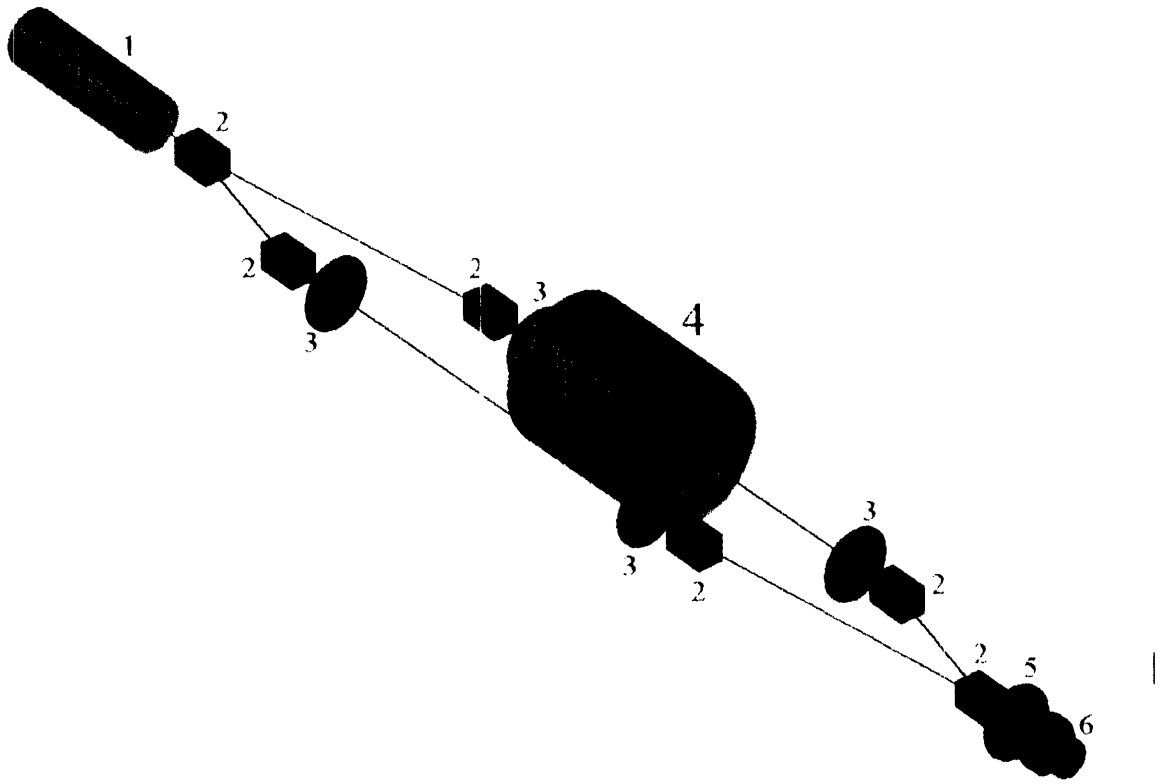

Figure 4.1. Lee-Woolsey polarisation interferometer

1 - He-Ne laser or 1.3 μm laser diode
2 - LF7/calcite prism
3 - lens
4 - thermally insulated invar tube
5 - polariser
6 - silicon or InGaAs photodiode

The gas under study was maintained in an invar tube placed in one arm of the interferometer. The 7 mm diameter tube was thermally insulated by surrounding it with a

thick layer of insulwool and by using double quartz windows on each end. Six chromel/alumel thermocouples were positioned along the length of the invar tube to monitor spatial and temporal variations in temperature. Variations in temperature within the tube were found to be less than 0.1 K during all series of measurements. The internal length of the tube was 486.42 mm. The gas pressure in the tube was measured using a VAISALA PTB200 A digital barometer, connected to a computer through a serial port. The VAISALA PTB200 A digital barometer uses a BAROCAP® silicon capacitive absolute pressure sensor. The barometer has 3 outputs: RS 232C full duplex serial interface, TTL level bidirectional serial output and a pulse output. The RS 232C serial output gives the best precision. The total accuracy is 20 Pa in the range 60000 Pa to 110000 Pa. The purities of the gases used were SF_6; 99.9%, and SOF_2; 98.5%. Light sources used were a He-Ne laser for 632.99 nm (the vacuum wavelength) and a laser diode for 1300 nm. A UDT 10DP silicon p-i-n photodiode was used for measurements at 632.99 nm and an EG&G C30642E InGaAs photodiode for those at 1300 nm. Photodiode signals were amplified and stored on computer after A/D conversion. The A/D converter is part of the acquisition card CONTEC ADC-10. The A/D converter has a 12 - bit resolution and maximum speed of 30000 samples per second. The whole interferometer arrangement was shielded to minimise convective air flow and to improve thermal stability. With this arrangement, it was possible to measure changes in optical path equivalent to 0.01 fringe at 632.99 nm and 0.05 fringe at 1300 nm.

4.1.3. The measurement procedure

The following procedure was adopted for making measurements. The invar tube was first evacuated to a pressure of less than 1 Pa. It was then filled with gas at a rate of about 30 Pa per second, and, as the pressure was increased from 60 kPa to 110 kPa, the pressure was recorded by the computer for each half fringe shift. There are about 1000 pairs of data (pressure and fringe shift) per measurement for SF_6 at 632.99 nm and half of that at 1300 nm. A second set of data was obtained as the gas was pumped from the invar tube. During the measurement, the rotary vane pump (figure 4.2) was switched off in order to avoid vibrations produced by the pump. Once the tube was filled with the gas, the pump was not

needed. For measurements made as the gas was removed from the tube, initially a nitrogen trap was used. However, the vacuum produced in the system between the needle valve NV1 (in figure 4.2) and the rotary vane pump by the same pump, was enough to lower the gas pressure in the tube below 60 kPa even when the rotary vane pump had been switched off. The procedure for the pumping out measurement was the following: the needle valve NV1 was closed and the rotary vane pump allowed to evacuate the volume between the pump and the needle valve, the pump was then switched off and the valve NV1 opened. This allowed the gas from the invar tube to slowly bleed into the evacuated part of the system. In this way the pressure in the invar tube varied from 120 kPa to 55 kPa.

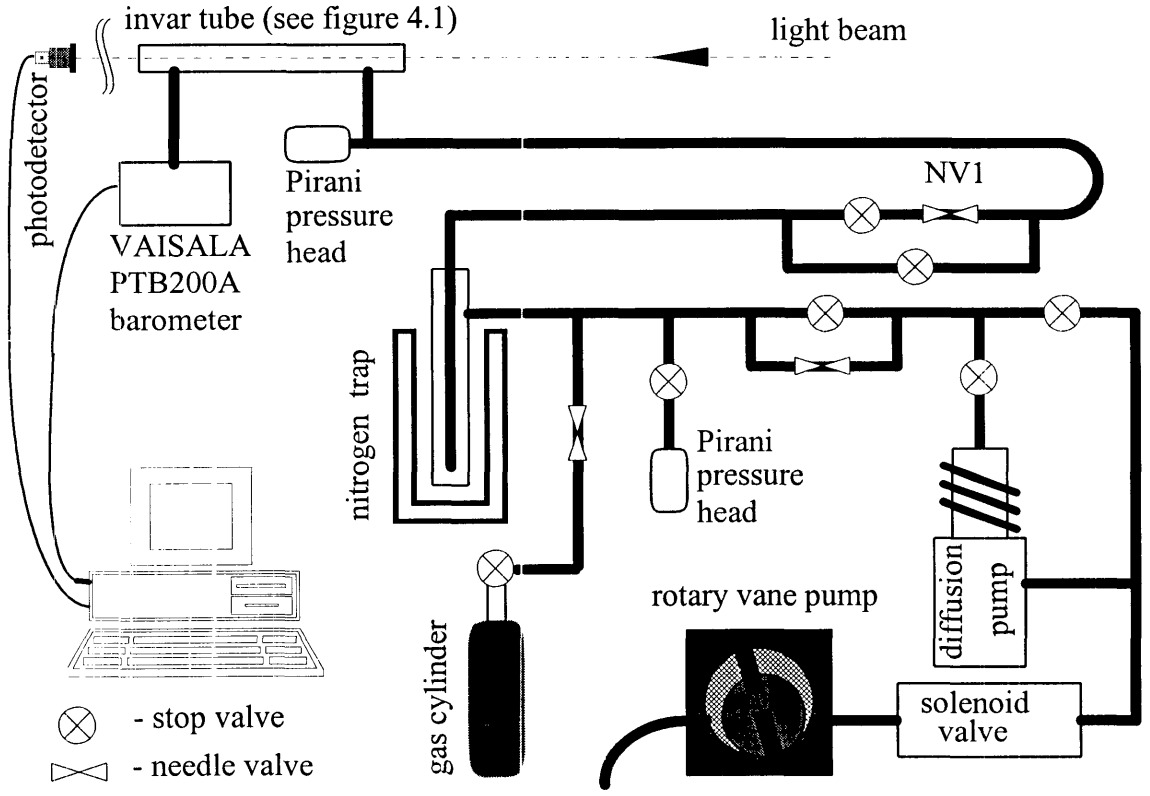

Figure 4.2. The vacuum section of the experimental arrangement for measuring refractive index.

An appropriate computer program and driver for the A/D converter were written for acquisition during the filling of the tube and a second program written for

evacuation. The programs are described in appendix 2. Fringe shifts were converted to refractivities using the equation

$$n - 1 = \frac{m\lambda_0}{L} \tag{4.12}$$

where m is the experimental fringe shift, λ_0 is the source wavelength in vacuum and L is the length of gas intercepted by the interferometer beam. The refractivity as a function of pressure and temperature can be fed into equation 4.4 to provide values for the coefficients A and $B(T)$. Then a curve of the form of equation 4.4 was fitted to a plot of refractivity as a function of pressure to provide values for the coefficients A and $B(T)$ for comparison with published data. A_R can be determined from equation 4.10, and $B_R(T)$ from equation 4.11. In order to calculate $B_R(T)$, a value is required for $B_p(T)$ at 25 °C, and this was determined by linear interpolation of the experimental data of Hamann *et al.* (1953) obtained at 20 °C and 30 °C.

Refractivities and refractive indices for different temperatures and pressures were calculated using equation 4.4. Although measurements were made at temperatures between 20 °C and 25 °C, all refractivity values were converted to 25 °C and one atmosphere, for comparison with published data. Equation 4.2 was used over this temperature range with $B(T)$ assumed constant. $B(T)$ does depend on temperature according to the relation (Thomas and Tayag, 1988)

$$B(T) = B_{295}\ \exp\left[T^* \left(\frac{295}{T} - 1 \right) \right] \tag{4.13}$$

where T^* is a constant for a specific gas, and for SF_6, is 4.20. However, the total variation in $B(T)$ between 20 °C to 25 °C, is only 3%, and because the contribution of the second term on the right-hand side of equation 4.4 is 100 times less than the contribution of the first term, $B(T)$ can be assumed to be constant over this temperature range. Indeed, the overall

uncertainty in the measured refractivities resulting from this assumption is 2.5 x 10^{-7}, which is less than the precision of the experiment.

4.1.4. The refractive indices of SOF_2 and SF_6

The results for refractivity and the various coefficients for both SF_6 and SOF_2 are given in Table 4.1 (633 nm) and Table 4.2 (1300 nm). The results of the present study are compared with those obtained in previous work in Table 4.3.

632.99nm	refractivity x10^6 @101325 Pa	refractivity x10^6 at 25 °C @101325 Pa	the first refractive virial coefficient A_R ($10^{-6}m^3/mol$)	coefficient A ($10^{-5}m^3/mol$)	coefficient B ($10^{-10}m^6/mol^2$)
SF_6	708.05±0.5 @ 22.9 °C	702.96±0.5	11.336±0.008	1.7005±0.0012	47.3 @ 22.9 °C
SOF_2	626.2±0.5 @ 22.8 °C	621.66±0.5	10.002±0.007	1.5004±0.0011	50.2 @ 22.8 °C

TABLE 4.1. Refractivity and refractivity virial coefficient at 632.99 nm for SF_6 and SOF_2

1300nm	refractivity x10^6 @101325 Pa	refractivity x10^6 at 25 °C @101325 Pa	the first refractive virial coefficient A_R ($10^{-6}m^3/mol$)	coefficient A ($10^{-5}m^3/mol$)	coefficient B ($10^{-10}m^6/mol^2$)
SF_6	698.7±1 @ 21.8 °C	694.0±1	11.18±0.016	1.676±0.0024	52 @ 21.8 °C
SOF_2	618.9±1 @ 22.8 °C	614.7±1	9.934±0.015	1.490±0.023	34 @ 22.8 °C

TABLE 4.2. Refractivity and refractivity virial coefficient at 1300 nm for SF_6 and SOF_2

The experimental uncertainties in the tabulated values include contributions from uncertainties in the measurements of fringe number, tube length, temperature and pressure. Since each interferometric measurement involved a total fringe shift of greater than 100, and these could be made to better than 0.01 fringe at 632.99 nm and 0.05 fringe at 1300 nm, the interferometric contributions to uncertainties are less than 0.01% and 0.05%

respectively. For the measurement at 1300 nm there is an uncertainty in the measurement of the wavelength of the laser diode of 0.03%. The uncertainty in the length of the invar tube is 0.01%. Pressures could be measured to within 20 Pa over the range of 60 kPa to 110 kPa, corresponding to an uncertainty of 0.03%. Temperatures were measured within 0.1 K, again corresponding to an uncertainty of 0.03%. No uncertainties are quoted in the tables for the coefficient $B(T)$, because, even with the degree of precision achieved, the uncertainties in the values of $B(T)$ are estimated to be as high as 100%. This is essentially because $B(T)$ is around 100 times smaller than A. However, since the nonlinear term in equation 4.4 is not significant at pressures around 1 atm and room temperature, the value of refractivity depends little on $B(T)$. Values for $B_R(T)$ are not presented in Tables 4.1 and 4.2, because, apart from depending on $B(T)$, $B_R(T)$ depends on B_p, values for which vary by more than 10% among different investigators (Hamann *et al.*, 1953; Clegg *et al.*, 1955; MacCormack and Schneider, 1951).

	refractivity x 10^6 at 25 °C @101325 Pa	coefficient A ($10^{-5}m^3/mol$)	the first refractive virial coefficient A_R ($10^{-6}m^3/mol$)	the second refractive virial coefficient B_R ($10^{-12}m^6/mol^2$)	coefficient B ($10^{-10}m^6/mol^2$)
This work	702.96±0.5	1.7005±0.0012	11.336±0.008		47.3 @ 296.05K
Buckingham and Graham, 1974	704.005 calculated*	1.701 calculated	11.34	29±5.4 @ 298K	48 @ 298K calculated*
Watson and Ramaswamy, 1936	699.39 @ 644.024nm				
St-Arnaud and Bose, 1979		1.7022 calculated	11.348±0.021 @ 323K	36±1.8 @ 323K	

TABLE 4.3. Comparison table for SF_6 at 632.99 nm

*Calculations were made using equations 4.3, 4.4 and 4.5 and knowing values for A_R and B_R. The value for B_p was obtained using linear interpolation of values given by Hamann *et al.*, 1953, B_p=-284.45·10^{-6} m^3/mol.

4.2. The refractive index in the SF_6 discharge

4.2.1. The refractive index in a corona discharge

In order to verify that the refractive index of the gas mixture in an SF_6 corona discharge does indeed decrease with discharge time, the following experimental procedure was carried out :

(i) The corona chamber was filled with SF_6 to a pressure of 1.8 atm. This value was chosen to allow for the fact that the upper pressure limit of the chamber is 2.0 atm, and the total pressure rises during the discharge.

(ii) A refractive index measurement was made with the polarisation interferometer after transferring gas from the chamber to the invar measuring tube. In order to obtain satisfactory precision for the measurement, the pressure in the invar tube needed to be at least 110 kPa (1.08 atm). As a result, each measurement decreased the pressure in the chamber by around 0.25 atm.

(iii) Further refractive index measurements were made in the same way until the pressure in the corona chamber fell to a value (1.2 atm) where the invar tube could no longer be filled to the required 1.08 atm.

In an experiment lasting 24 days, three measurements of refractive index were possible. These are plotted in the graph of Figure 4.3, together with the initial value. The graph shows that there is a steady fall in refractive index as the corona discharge proceeds.

This fall in the index of refraction suggests that it may be possible to measure the degradation of SF_6 in a high - voltage system by measuring the refractive index of the insulated gas. For the same initial conditions in a particular system, it might be expected that partial discharge activity in a high-voltage would always cause SF_6 degradation to follow a similar path. That is, following the passage of a given amount of charge through the system, the concentrations of the various by-products would be somewhat similar. In practice, this method would require obtaining a calibration curve for a specific device, similar to that of figure 4.3. When the refractive index is measured it should be normalised for pressure and temperature. It means that each device needs precise sensors for measuring pressure and temperature and these need to be built into the high-voltage device.

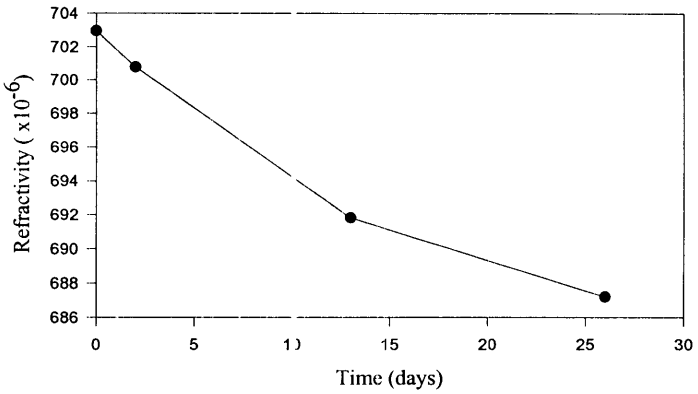

Figure 4.3. The index of refraction of the mixture of gases during a corona discharge. The discharge current is 20 μA; distance between electrodes (point and plane) is 10 mm; initial pressure of SF_6 was 1.8 atm.

4.2.2. A practical monitoring system

In order to measure the index of refraction in a high voltage SF_6 - insulated device in the field, gas cannot be moved in and out of the system. It is necessary, therefore, to use white light interferometry rather than the monochromatic interferometry described earlier. Since a white light interferometer does not need initialising it can be used to monitor the high-voltage device continuously. There are many different kinds of white light interferometer and these are discussed in chapter 8.

4.3. Determination of separate gas concentration

A possible extension of the experimental measurement described here would be a measurement of the separate concentrations of all the species in the degraded SF_6 gas mixture. In principle, this can be done using measurements of the refractive index of the mixture at different wavelengths together with data on the refractive indices of the constituent gases at these same wavelengths. In order to carry out such an analysis the gas pressure has to be sufficiently low, so that the non-linearity of the refractive indices can be neglected.

Under these ideal conditions, a gas mixture may be considered as being made of layers of constituent gases, as illustrated in figure 4.4. for a three - gas mixture. In figure 4.4.(a), a mixture of 3 gases is assumed to exist in a dielectric cylinder contained between a pair of metal electrodes. If the cross-sectional area of the cylinder is S and the length is L, the electrical capacitance between electrodes is

$$C_m = \frac{\varepsilon_0 \varepsilon_m S}{L} \tag{4.14}$$

where ε_0 is the dielectric constant of vacuum and ε_m is the relative dielectric constant of the gas mixture.

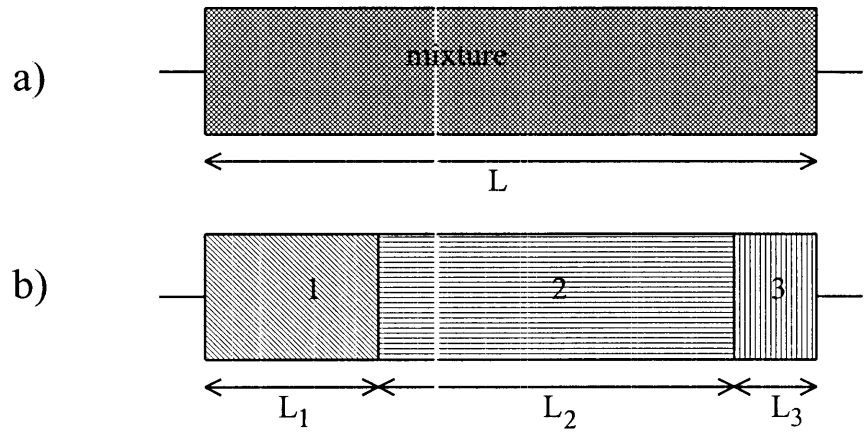

Figure 4.4. For linear gases the capacitance of a cylinder filled with mixture of 3 gases is the same as the capacitance of 3 capacitors in series where the gases from the mixture are separated in 3 capacitors.

The overall capacitance C_m is equivalent to three capacitors connected in series, with

$$\frac{1}{C_m} = \frac{1}{C_1} + \frac{1}{C_2} + \frac{1}{C_3} \tag{4.15}$$

where C_1, C_2 and C_3 represent the capacitances of the separate layers of gas, and

$$C_1 = \frac{\varepsilon_0 \varepsilon_1 S}{L_1} \tag{4.16}$$

where ε_1 is the relative dielectric constant of gas 1, and there are similar relations for C_2 and C_3. Substituting the expressions for C_1, C_2, C_3 and C_m into equation 4.9 as well as

$$L = L_1 + L_2 + L_3 \tag{4.17}$$

gives

$$\frac{1}{\varepsilon_m} = \frac{K_1}{\varepsilon_1} + \frac{K_2}{\varepsilon_2} + \frac{K_3}{\varepsilon_3} \tag{4.18}$$

where K_1, K_2 and K_3 are the concentrations of the gases and

$$K_p = \frac{V_p}{V_m} = \frac{L_p S}{L S} \tag{4.19}$$

where V_p and L_p are the volume and the length of gas p, and V_m is the overall volume. For gases

$$\varepsilon = n^2 \tag{4.20}$$

and equation 4.18 becomes

$$\frac{1}{n_m^2} = \frac{K_1}{n_1^2} + \frac{K_2}{n_2^2} + \frac{K_3}{n_3^2} \tag{4.21}$$

If n_{pq} is the refractive index of gas p at wavelength q, a system of linear equations can be written such as

$$\frac{1}{n_{m1}^2} = \frac{K_1}{n_{11}^2} + \frac{K_2}{n_{21}^2} + \frac{K_3}{n_{31}^2} \tag{4.22}$$

$$\frac{1}{n_{m2}^2} = \frac{K_1}{n_{12}^2} + \frac{K_2}{n_{22}^2} + \frac{K_3}{n_{32}^2} \tag{4.23}$$

$$K_1 + K_2 + K_3 = 1 \tag{4.24}$$

n_{11}, n_{21}, n_{31} and n_{m1} are the refractive indices of gases 1, 2 and 3 and the gas mixture in the cylinder, respectively, at the first wavelength.

n_{12}, n_{22}, n_{32} and n_{m2} are the refractive indices of gases 1, 2 and 3 and the gas mixture in the cylinder, respectively, at the second wavelength.

Hence the values of the gas concentrations K can be determined from a series of measurements of the refractive index of the gas mixture at different wavelengths, n_{m1}, n_{m2}, ..., if the refractive indices of the individual gases are known at the same wavelengths. Measurements must be made at $(g\text{-}1)$ wavelengths, where g is the number of gases in the mixture. Because the differences between refractivities are small, the refractive indices are very close to 1, and the changes in refractive index with wavelength for one gas are small, measurements must be made with a precision of at least $1\text{x}10^{-7}$ with, for example, a refractometer of the type described by Kerl and Jescheck (1982). With this interferometer it is possible to obtain the refractive indices of a gas in the whole visible spectrum during one measurement. Also, calculations must be made with high precision. On some computers, where floating-point calculations are carried out with 12 significant digits, which is equivalent to 40 bits, an error can be accumulated during the calculation. For example, there would be a difference between

$$\frac{n_{11}n_{21} + n_{11}n_{31} + n_{21}n_{31}}{n_{11}n_{21}n_{31}} \tag{4.25}$$

and

$$\frac{1}{n_{11}} + \frac{1}{n_{21}} + \frac{1}{n_{31}} \tag{4.26}$$

The second calculation is less accurate than the first one because more divisions are involved. Larger errors occur in calculations involving division than those involving multiplication, subtraction and addition.

The measurement procedure described here for a mixture of three gases can be extended to any number of gases in the mixture.

As discussed earlier, a monitoring procedure for concentrations of individual species based on the measurement of refractive index at different wavelengths requires refractive indices to be measured with a precision of 1×10^{-7}. The precision available with the measuring system used here is restricted to 5×10^{-7} at 632.99 nm. It was decided therefore not to extend the refractivity analysis in this manner as part of the present program, although it is an approach that could be considered in future, if a more precise system becomes available for the measurement of refractivity.

4.4. Improvement of the Lee-Woolsey Interferometer

It can be seen in figure 4.1 that the interferometer arrangement includes a polariser in front of the detector. The prism in front of the polariser combines two beams that are orthogonally polarised. They are orthogonally polarised when they enter the polariser, which has to be rotated in order to obtain fringes. If the two beams have the same intensity, the transmission axis of the linear polariser should be at 45° with respect to both beams. The best fringe contrast is obtained when the two beams have equal intensity. The equal intensity can be achieved by rotating the laser. But the laser and the polariser have to be rotated simultaneously. The arrangement can be simplified if a quarter-wave plate is placed in front of the linear polariser. Then the fringes appear without adjustment of the polariser and it is easy to set the maximum contrast by rotating the laser. The fast axis of the quarter-wave plate must be at 45° to the direction of the transmission axis of the linear polariser, and that is assumed in further discussions. This combination of quarter-wave plate and linear polariser also is often

used as an optical isolator to prevent feed-back into a laser, but with the optical components reversed.

4.4.1. Matrix Treatment

Jones vectors can be used to analyse the interferogram produced when a quarter-wave plate is placed in front of the linear polariser in figure 4.1.

The Jones matrix for a quarter-wave plate with vertical fast axis (along the y-axis) is given by (Gerrard and Burch, 1975)

$$\exp\left(-i\frac{\pi}{4}\right)\begin{pmatrix} 1 & 0 \\ 0 & i \end{pmatrix} \tag{4.27}$$

and for a linear polariser, with transmission axis at 45° with respect to the y-axis, the Jones matrix is

$$\frac{1}{2}\begin{pmatrix} 1 & 1 \\ 1 & 1 \end{pmatrix} \tag{4.28}$$

When these two plates are in series with the light first passing through the quarter-wave plate, the resultant matrix is

$$\frac{1}{2}\exp\left(-i\frac{\pi}{4}\right)\begin{pmatrix} 1 & i \\ 1 & i \end{pmatrix} \tag{4.29}$$

The Jones vector for a linear polarised beam at an arbitrary angle α with respect to the y-axis (see figure 4.5) is given by

$$E\begin{pmatrix} \sin\alpha \\ \cos\alpha \end{pmatrix} \tag{4.30}$$

where E is the amplitude.

In order to find the output light, the Jones matrix of the plates (equation 4.29) has to be multiplied by the input beam matrix (equation 4.30). The result is:

$$E_1 = \frac{1}{2}E(\sin\alpha + i\cos\alpha)\exp\left(-i\frac{\pi}{4}\right)\begin{pmatrix}1\\1\end{pmatrix} = \frac{1}{2}E\exp\left[-i\left(\frac{\pi}{4}-\alpha\right)\right]\begin{pmatrix}1\\1\end{pmatrix} \qquad (4.31)$$

For a beam orthogonally polarised to this beam the angle α is replaced by $\alpha+\pi/2$ and the equation for the orthogonally polarised beam with respect to the beam described by equation 4.31 is obtained by substituting α with $\alpha+\pi/2$. For an equal amplitude beam it gives

$$E_2 = \frac{1}{2}E(\cos\alpha - i\sin\alpha)\exp\left(-i\frac{\pi}{4}\right)\begin{pmatrix}1\\1\end{pmatrix} = \frac{1}{2}E\exp\left[-i\left(\frac{\pi}{4}+\alpha\right)\right]\begin{pmatrix}1\\1\end{pmatrix} \qquad (4.32)$$

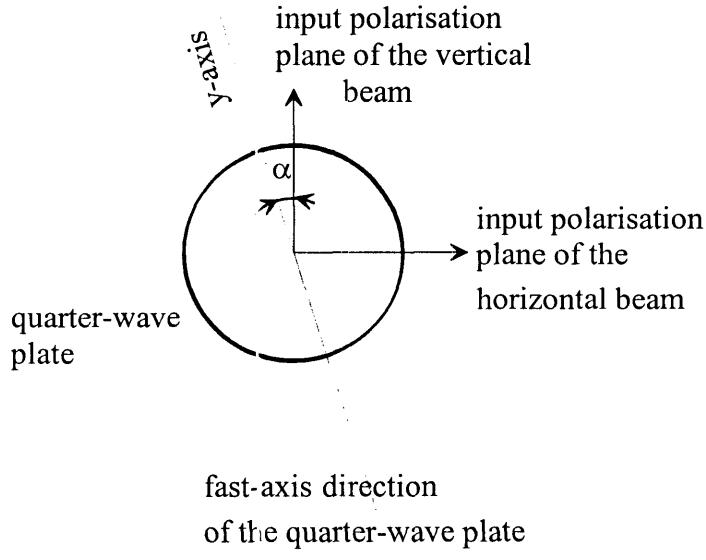

Figure 4.5. Input orthogonally polarised beams and their positions with respect to the fast axes of the quarter-wave plate.

The beams represented by E_1 and E_2 have the same amplitude and are linearly polarised at 45° to the x-axis. There is a phase difference of $\pi/2$ between them. The two beams will interfere to provide an interference pattern. It is clear that maximum contrast occurs when the two beams have equal amplitudes, and this is achieved by rotating the laser source. When the quarter-wave plate is omitted, maximum contrast requires appropriate rotation of the laser and linear polariser.

4.5. Summary

This chapter has examined the possibility of using measurements of refractive index as a means of optically probing SF_6 degradation in high-voltage, SF_6 - insulated systems. A possible method has been explored experimentally, and preliminary data suggest that it is feasible. This method relies on the fact that the refractive index of SF_6 is high. It is higher than the refractive indices of the major by-products in a high voltage discharge. This means that the loss of SF_6 as a result of production of other species can be observed as a fall in the refractive index of the SF_6 - discharge gas mixture with time. This was verified by measuring the refractive index of the gas mixture in a corona discharge maintained over several days. One of the dominant by-products is SOF_2. A new measurement has been made of the refractive index of SF_6 at 632.99 nm. The result is in agreement with previously published data. Using the same apparatus, the refractive index of SOF_2 was measured at 632.99 nm for the first time. The refractive indices of SF_6 and SOF_2 at 1300 nm also were measured for the first time. These measurements show that the refractive index of SF_6 is higher than the refractive index of SOF_2.

The measurements showed a steady fall in the refractive index of the discharge gas during the corona discharge. Therefore, such measurements of refractive index in high voltage systems have the potential to be used for monitoring SF_6 - insulated devices.

Measuring the refractive index of a gas mixture at several wavelengths has potential for measuring the concentration of each gas in the mixture. The method has some limitations: the most significant is that very high precision measurements are required.

Chapter 5

Review of chemical optical fibre sensing

5.1. Optical fibre sensors

The developments in optical fibre sensing during the past decade show that optical fibre sensors have great potential. They have better sensitivity than many existing sensing techniques and they can be made very compact and insensitive to their environment. Their dielectric characteristic makes them ideal for use in situations involving high voltage, electromagnetic and electric noise, and corrosive materials. Another important advantage is in multiplexing. It is relatively easy to combine, transmit and extract information from several measuring points through the same fibre. They can be used to replace almost all classical sensors. Up to the present, commercial exploitation has been limited, but a few have achieved commercial success, such as the Luxtron 1000 temperature sensor based on temperature -dependent phosphorescence (Grattan, 1990).

Optical fibre sensors can be divided into two types: intrinsic and extrinsic. In an intrinsic sensor, light does not leave the fibre and the sensing signal is the result of modulation of the light while it travels through the fibre due to changes produced in the fibre core or cladding (or surrounding medium if there is no cladding) by changes in the quantity being measured. An example of an intrinsic sensor is an evanescent-field optical fibre sensor where the medium that surrounds the core (figure 5.2) causes attenuation of the light that propagates through the fibre. Fibres in extrinsic sensors are used to transmit and receive light that is modulated by the measurand when it is external to the fibres. In some cases, the light can be produced in some other way and the fibre is used simply to collect the light and transmit it to the detector. An example of an extrinsic sensor is shown in figure 5.1. The

chemical compound in the reflector changes its optical properties when it reacts with the measurand. Light that is collected in the detecting fibre depends on these changes. Thus, the detected light is modulated by the chemicals that react with the reflector.

According to which component of the light-wave function (equation 5.1) is modulated by the quantity being measured, optical fibre sensors can be divided into interferometric (phase), polarisation - modulated, frequency - modulated and amplitude - modulated sensors. The electric vector of an electromagnetic wave can be written as:

$$\mathbf{E} = \mathbf{E}_0 \sin(\omega t - kx + \varphi) \tag{5.1}$$

Interferometric sensors are based on modulation of the phase difference φ between two light waves. These sensors are very sensitive. An example of this high sensitivity of interferometric sensors is seen in the interferometric acoustic sensor (Cole *et al.*, 1977; Bucaro *et al.*, 1977). The sensitivity of this sensor, using a 1 m length of plastic-coated optical fibre, is equal to the sensitivity of a state-of-the-art piezoelectric sensor. The sensing length of the plastic-coated optical fibre can be increased to increase the sensitivity further. Using a 1000 m length, the sensitivity increases by 55 dB (Bucaro and Hickman, 1979).

Modulation of wavelength (propagation constant, k) and frequency are also used in sensor design and all fluorescent and phosphorescent-based sensors described in the next section use wavelength modulation. Amplitude-based and frequency-modulated optical fibre sensors are not as sensitive as interferometric sensors. Light is launched into the sensor fibre at one wavelength and fluorescent or phosphorescent light is collected at a different wavelength. The amplitude of the output light decreases as light is absorbed through evanescent-field interaction with the material surrounding the core. Such a sensor can be used to measure the concentration of a chemical that surrounds the fibre when monochromatic light is transmitted through the fibre (see chapter 7). For measuring the concentration of several compounds, in a fluid which is a mixture of few compounds, a broad-wavelength band light is more appropriate. When it is transmitted through the fibre, an output spectrum can be obtained and an analysis carried out to determine the concentrations in the mixture.

An external influence on an optical fibre, such as a magnetic field, can change the polarisation vector of transmitted light and this form of modulation can be used in sensor design (Park *et al.*, 1996).

5.2. Chemical sensing

The optical fibre sensing techniques used in this study are chemical. Many of the established chemical sensing and analysing techniques that use bulk optics can be employed with optical fibres; these include fluorescence, phosphorescence, chemiluminescence, evanescent-wave absorption, internal reflection spectroscopy, ionic indication, absorption, opto-mechanical effects and FTIR (Fourier Transform Infrared Spectroscopy). The process used here for sulphur measurement relies on evanescent-wave absorption, but it is useful to review some of the other optical methods that have been applied to chemical sensing using optical fibres.

5.2.1. Luminescence

When energy is absorbed by a substance it can be re-emitted, usually with less energy than the input energy. The input energy excites atoms or molecules which may radiate when they return to a lower energy state. Otherwise they can lose the energy in thermal collisions. Excitation may occur through photoluminescence (excitation by light), thermoluminescence (excitation by heat), chemiluminescence (excitation by chemical reaction) or electroluminescence (excitation by electric field or current).

Energy re-emission may take place through fluorescence or phosphorescence, which are essentially special forms of light scattering: light comes from one direction and is re-emitted in random directions with a longer wavelength. The difference between these two processes is in the way in which the atoms or molecules return to the lower energy state. The time between absorption and emission for fluorescence is less than 10^{-8} s (Dakin and Culshaw, 1988), while for phosphorescence the time is substantially longer.

In fluorescence, an excited atom, molecule or ion emits the light shortly after absorption. When a molecule is in an excited state it may exist in one of many very close vibration states within the first excited state. It can lose a small amount of energy in thermal collisions by moving from one vibration state to another before it returns to the ground state. Because of that, the peak of the emitted spectrum is shifted towards a longer wavelength relative to the absorption wavelength.

Phosphorescence represents a similar effect. A condition for the existence of phosphorescence is that there is a triplet state, close below the first excited singlet state, into which the molecule can fall. Then a transition from this triplet state to the lower energy, usually ground state, occurs. It involves a forbidden triplet → singlet jump, and because this transition is not absolutely forbidden, the transition does finally occur but the process is relatively slow. Because of the low probability of the transition, the molecule remains for a relatively long time in this so-called metastable state before radiative emission occurs. So, for phosphorescence, the time between absorption and emission is much longer (milliseconds) than for fluorescence.

These mechanisms can be employed for optical fibre sensing in many ways. The Luxtron 1000 temperature sensor, for example, is based on the temperature-dependent phosphorescence of rare-earth phosphors (Dakin and Culshaw, 1988). The emission intensity varies with time according to

$$I = I_0 \exp\left(-\frac{t}{\tau}\right) \tag{5.2}$$

where I is the intensity of phosphorescent light, I_0 is the initial intensity of phosphorescent light, t is time and τ is a temperature-dependent constant. For this sensor a piece of rare earth phosphor is placed on the tip of an optical fibre. The same fibre delivers UV light to the piece of phosphor and collects the phosphorescent light. The Luxtron 1000 measures the intensities of the UV light and phosphorescent light. The temperature is determined from the ratio of these two values. The later version Luxtron 750 does not measure the intensity of the UV light source. For this measurement, the intensity of the phosphorescent light as a function of time is

recorded and the decay constant (τ) is calculated. The temperature is determined from this temperature-dependent constant. The light source is pulsed. The phosphorescent material used in the Luxtron sensor is magnesium fluorogermanate (Grattan, 1990).

During fibre manufacture, fluorescent material can be added. Such a fibre can be used, for example, to detect a corona discharge inside a high-voltage device filled with SF_6 (Farenc *et al.*, 1994). Light produced by a corona discharge in SF_6 has peak emission between 460 nm and 500 nm (Casanovas *et al.*, 1991). A phosphorescent material with absorption within this range is mixed with polystyrene to produce a plastic optical fibre. When the optical fibre is placed in a high voltage device filled with SF_6, light produced by a corona is absorbed by the optical fibre. Phosphorescent light is produced within the optical fibre and this light is radiated in all directions. Some of the light is trapped in the optical fibre and transmitted along the fibre out of the device to a detector. The output signal depends on many parameters: the nature of the phosphorescent material, its concentration, the length of the optical fibre, the quality of the fibre end, the sensitivity of detector, and the position of the fibre in relation to the corona source. It is reported that with carefully chosen parameters it is possible to produce useful signal after the photodetector of up to 50 mV from a 10 cm length of fibre exposed to light from an AC corona discharge, 2 5 cm away from the corona source, which is a point/plane electrode system in SF_6 atmosphere (Farenc *et al.*, 1994).

An optical fibre can be coated with a fluorescent or phosphorescent substance using a sol-gel process. A sol-gel derived coating is porous and traps molecules, which increases the concentration of measurand species (gas or liquid) in the coating. This makes a sensor more sensitive. A compound that reacts with the measurand is mixed with the coating during the sol-gel process. Light is absorbed in the coating via the evanescent field and a fraction of the resultant fluorescent or phosphorescent light is coupled into the fibre. The measurand species that surrounds the fibre is trapped in the sol-gel coating, and reacts with the substance embedded in the coating. This reaction produces the optical effect that can be monitored to provide quantitative information of the concentration of measurand species. For example, oxygen quenches the fluorescence of a ruthenium complex and it is used for oxygen sensing. The ruthenium complex fluoresces yellow when it is irradiated with blue light. The

ruthenium complex can be a part of sol-gel coating. In this case a part of the emitted light is coupled into the measuring fibre and transmitted along the fibre. It can be measured if the strong incident blue light is blocked with a cutoff filter at 505 nm. Oxygen quenches this fluorescence and the light intensity at the output of the fibre decreases as the concentration of oxygen increases. The light source can be a laser (MacCraith *et al.*, 1993) or an LED (MacCraith *et al.*, 1994).

When light is absorbed in a semiconductor, electrons from the valence band move to the conducting band, so that electron-hole pairs are generated. These electrons can lose their energy by thermal collisions or by a radiative transition (photoluminescence). When an n-type semiconductor is coated with a metal, a Schottky barrier junction is formed. A Schottky barrier junction is similar to a p-n junction except that it is a metal - n-type semiconductor junction where the metal acts as an anode and the semiconductor as a cathode (Sah, 1991). An important feature of this junction is that the depletion region is much thinner than in a p-n junction. For optical purposes, it is made by coating a semiconductor with a thin metal (usually gold) film. The depletion region is just under the metal surface, so that light can penetrate through the metal layer, reach the semiconductor underneath and generate electron-hole pairs. The carriers produced in the depletion region do not emit light because the generated electrons and holes are driven away by the internal electric field of the junction, and the probability for their recombination is greatly reduced. Electrons are pushed into the semiconductor and holes into the metal. Only electrons and holes generated in the semiconductor, rather than in the depletion region, can cause photoluminescence. When the width of the depletion region is large, fewer electrons are generated outside this region and photoluminescence is weaker.

A sensor made from a Schottky barrier photodiode can be used for measuring the concentration of fluorine. A Schottky barrier photodiode made up of several monolayers (1×10^{-9} mol cm^{-2}) of redox-active sites on n-GaAs (Van Ryswyk and Ellis, 1986) and illuminated with argon laser light at 457.9 nm radiates light with a peak at 865 nm. When the sensor is exposed to volatile oxidants such as the halogens (F_2, Cl_2, Br_2 or I_2) the depletion width increases and hence the intensity of the 865 nm peak decreases. The photoluminescence

regains its original intensity when the sensor is flushed with N_2H_4. In order to make an optical fibre sensor for the study of the fluorine distribution in an SF_6 discharge, a Schottky barrier photodiode of this type could be bonded to an optical fibre with adhesive. The fibre would deliver laser light and receive photoluminescent light. Another possibility is to grow gallium arsenide on a sapphire optical fibre.

5.2.2. Absorption sensors

Optical fibre absorption sensors use all the features of absorption spectroscopy. Here, fibres are used to transmit light to a sample and to collect the reflected and attenuated light due to absorption. A classical arrangement is shown in figure 5.1. The reflector can be an appropriate transparent porous gel that traps targeted molecules. For example, an aqueous gel of Sephadex with a layer of haemoglobin can be used for sensing oxygen (Zhujen and Seitz, 1986). In the sensor of figure 5.1, only a small portion of the reflected light is collected, which makes measurements difficult and insensitive. A better solution is to use evanescent-wave absorption, which will be described in detail in section 5.2.3.

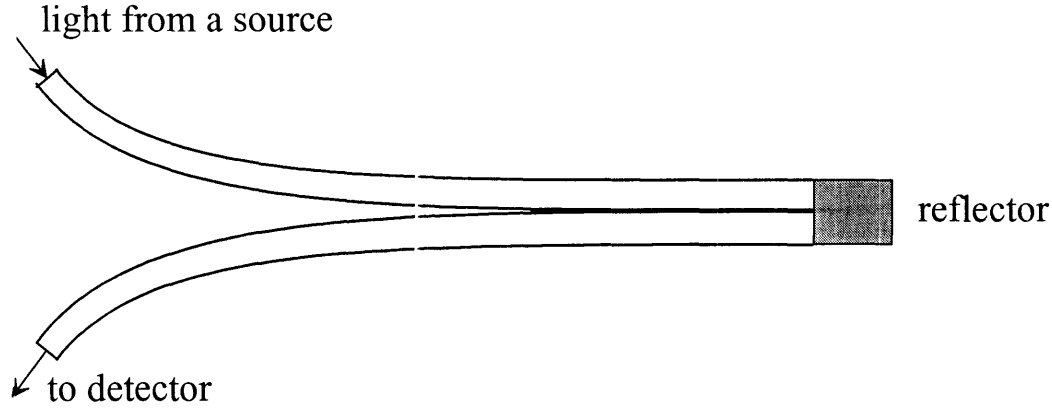

Figure 5.1. An optical fibre absorption sensor. Light is transmitted from a source to the reflector where it is absorbed. The reflected light is coupled and transmitted by a second fibre to a detector. The source can be monochromatic or white light.

5.2.3. Biosensors

In general, biosensors can be classified into those groups previously described for chemical sensors. However, they do have some special characteristics. Immunochemicals (antibodies) and enzymes, used in optical fibre biosensors, are very selective and this, together with high optical sensitivity and small probe dimensions, makes optical fibre biosensors the most selective of all chemical sensors. Enzymes catalyse chemical reactions that involve measurands. Products of the reaction affect the signal in the optical fibre. The change in the output signal can be due, for example, to a change in refractivity, absorption and luminescence. Antibodies are more selective than enzymes. They attract corresponding antigens that can be detected in many different ways. Immunochemicals and enzymes can be covalently attached to the core of the fibre after removing the cladding (Anderson *et al.*, 1994), or the core can be coated with enzymes or antibodies using a sol-gel process, or they can be placed inside the reflector of figure 5.1. The problem with antibody fibre optic sensors is that they become irreversibly saturated and so does the measured signal (Janata, 1989). The solution is to measure the rate of binding antigens with antibodies; that is, the differential of the optical signal. Another problem with biosensors is their short-term stability, as they can be used only for a few days. For example, the sensor made by Kunz *et al.* (1996) for detection of fatty acids can be used only for four days.

5.2.4. Evanescent field optical fibre sensors

These devices, sometimes also called FEFA (Fibre-optic-based Evanescent Field Absorption) sensors, rely on the following process. When an electromagnetic wave travels through an optical fibre, a part of the wave travels in the fibre cladding or whatever medium surrounds the fibre core. That part of the wave is called the evanescent field. The depth of penetration into the surrounding area is inversely proportional to the core diameter, and also depends on the difference in refractive indices between core and cladding. Normal optical fibres are designed in such a way that the light is mainly confined within the core and the evanescent field fades into the cladding. In order to expose the evanescent field to the surrounding medium a fibre can be tapered, for example, by heating up to the melting point

and stretching. The core and cladding become thinner and the total diameter can be reduced to less than 1 μm. As the diameter of the core decreases in the tapered region, the waveguide parameter of the fibre, or the *V*-number, defined as $V = \frac{2\pi}{\lambda}\rho\sqrt{n_{co}^2 - n_{cl}^2}$ (see Appendix 3) decreases, and the ratio of light power in the core to that in the cladding decreases. Depending on the shape of the tapered region one or more modes can be coupled into the cladding (Payne and Mackenzie, 1991). The intensity of the electric field of the light is depicted in figure 5.2 as a red net. If the evanescent field interacts with the molecules of the surrounding medium, the intensity of the light at the output of the fibre is reduced.

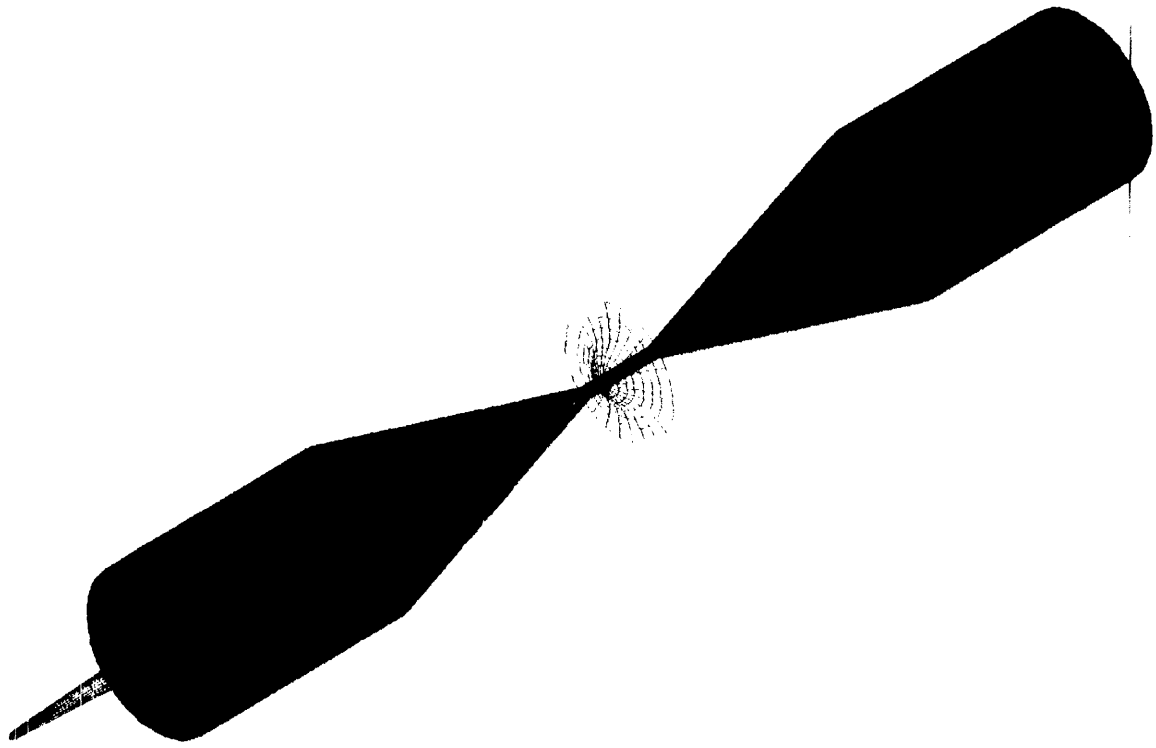

Figure 5.2. Tapered single mode optical fibre: blue is the cladding; green is the core; the amplitude of the red net represents the strength of the electric (and magnetic) field.

Light travelling through a tapered optical fibre, such as that depicted in figure 5.2 can be very sensitive to the surrounding medium. However, tapered fibres are very fragile and difficult to handle because the diameter of the core in the tapered region is typically around 2 μm (Henry, 1994A; Hale and Payne, 1994). The tapered region is usually a few millimetres long and it is difficult to make it longer. Increasing the length of the tapered

region improves the sensitivity, but this is difficult because of the fragile nature of such a fibre.

The sensitivity of a tapered optical fibre sensor based on evanescent - field interaction can be further increased by using a sol-gel-derived coating as described in section 5.2.1.

An alternative to the tapered optical fibre is the D-fibre (Stewart and Culshaw, 1994; Henry, 1994A) which is depicted in figure 5.3. The cladding is removed from one half of the fibre along the axis so that a section of the core is exposed to the surrounding medium. This configuration is not as sensitive (per unit length) as the tapered fibre but the mechanical strength is similar to that of a standard optical fibre. The sensitivity can be increased by extending the length of the fibre. A methane sensor using D-fibre has been developed using the methane absorption line at 1.66 μm (Muhammad and Stewart, 1992).

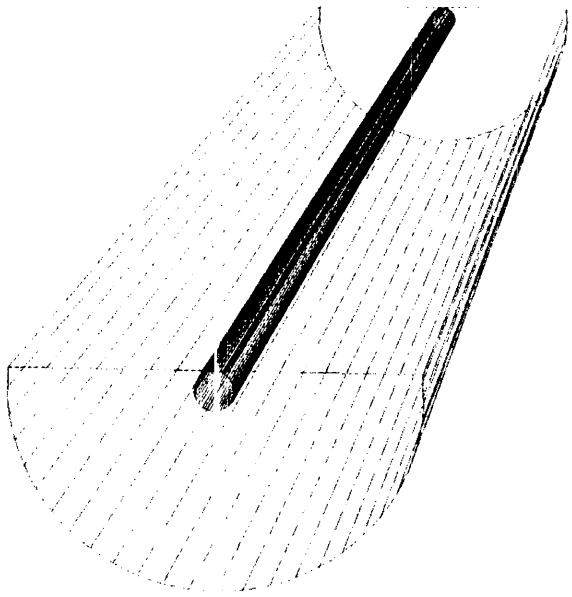

Figure 5.3. A section of a D-fibre. The red part is the core.

The sensitivity of sensors made with multimode optical fibres can be increased by launching the light with a high incident angle with respect to the fibre axis, as explained in section 5.2.3.2. For example, a tunable lead salt laser diode at around 10.6 μm was used as a light source to couple the light into a silver halide optical fibre in order to sense SF_6 (Messica

et al., 1994). When the light is launched at a high angle, a significant amount of light is reflected from the fibre end where the light is coupled in, so that the actual launching angle is a compromise. Messica *et al.* (1994) have found that, for the optimal result, the light should be launched at an angle of 20°. The output absorbance as a function of the pressure of SF_6 is shown in figure 5.4. The absorbance is the negative natural logarithm of normalised transmitted power.

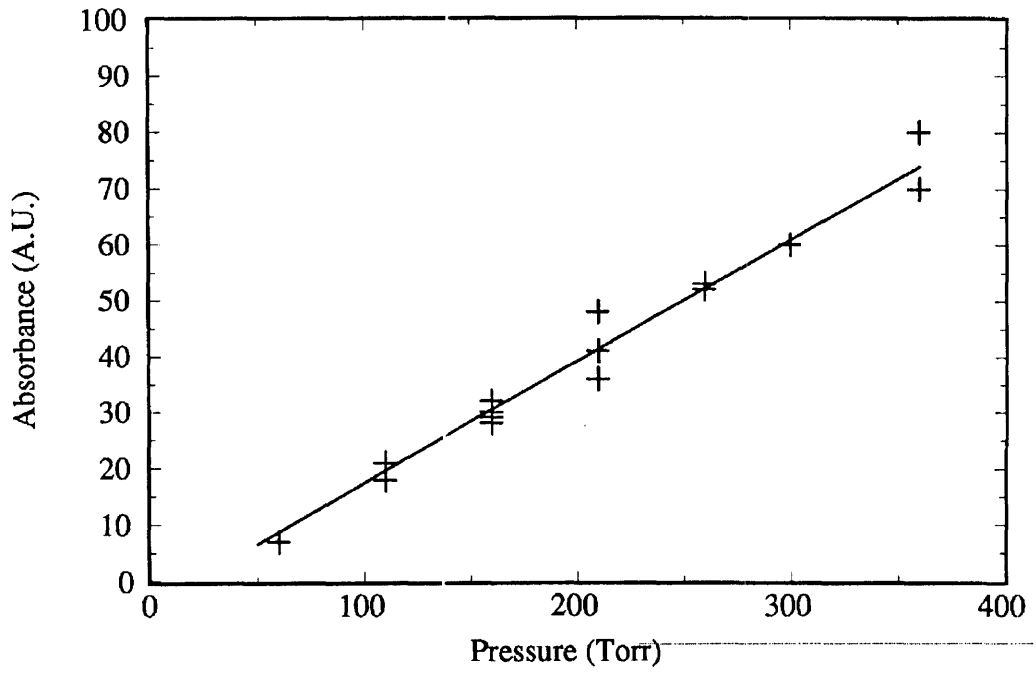

Figure 5.4. Evanescent wave absorption by SF_6. The absorbance is the negative natural logarithm of normalised transmitted power. It is shown as a function of the pressure of SF_6. A silver halide optical fibre without cladding was used and its diameter was 900 μm. The lead salt laser diode was tuned to 10.562 μm, which is the absorption peak of SF_6 (from Messica *et al.*, 1994).

The typical output power of a lead salt laser diode is around 1 mW. These diodes operate at cryogenic temperatures and are produced for wavelengths up to 30 μm.

5.2.4.1. Source-fibre coupling for FEFA sensors

As described in the previous section, for a large-diameter multimode fibre, the sensitivity of evanescent - wave interaction is increased by launching the light at a high incident angle with respect to the fibre axis. The penetration outside the core of the

evanescent-field of a meridional ray following a zigzag path is given in appendix 4 by equation A4.6. A meridional ray is a ray that crosses the axis of the fibre. When laser light is used, it can be launched as a narrow beam to trace a zigzag path within the fibre. Alternatively, a diverging coherent or incoherent light source can be used; for example, an LED or diverging laser beam. In order to compare the sensitivity obtained using the two types of sources, calculations for the power of the evanescent field for narrow and wide-beam sources are made for CO_2 laser light and a 1 mm thick silver halide optical fibre with the refractive index of 2.1 at 10.6 μm, as used in the experimental work described in chapter 7.

First a wide-angle source is considered. Because of the high V-number of large-diameter multimode fibres, a ray approach is appropriate (Schnitzer *et al.*, 1990). Equations A3.24 and A3.25 show that if a wide-angle source is used, the light propagates through the fibre with 149765 modes, and 0.34% of the total power transmitted through the fibre travels in the cladding as an evanescent wave. This calculation is for a lossless surrounding medium where the refractive index is 1.

Secondly a narrow zigzag beam is considered. An estimate of the power of the evanescent field when the laser beam follows a zigzag path inside the fibre can be made by assuming that the fibre is a planar waveguide. This is a good approximation for a thick (1 mm) fibre. Dispersion can be neglected. For a lossless dielectric waveguide between 2 identical dielectric planes (see figure 5.5.), the power of the evanescent wave is given by the equation (Kogelnik and Weber, 1974)

$$P_{clad} = \frac{1}{1+\rho q h_2} P_{tot} \tag{5.3}$$

where

ρ is the half width of the waveguide and

$$h_2 = n_{co}\frac{2\pi}{\lambda_0}\sin\theta_1 . \tag{5.4}$$

This is the same h_2 as defined in appendix 3.

λ_0 is the wavelength of the light in free space,

n_{co} is the refractive index of the waveguide dielectric,

θ_1 is the incident angle with respect to the direction perpendicular to the surface of the waveguide,

q is equal to 1 for TE modes, and for TM modes, it is given by

$$q = (n_{co}\sin\theta_1)^2\left(\frac{1}{n_{cl}^2}+\frac{1}{n_{co}^2}\right)-1 \qquad (5.5)$$

where n_{cl} is the refractive index of the dielectric surrounding the waveguide.

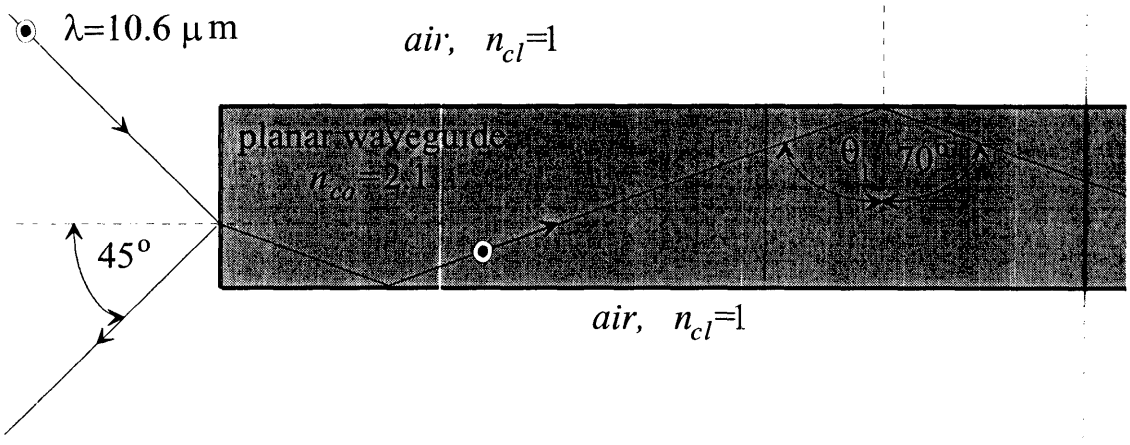

Figure 5.5. Light beam coupling (from CO_2 laser) into a 1 mm thick planar dielectric (silver halide) waveguide in air. The wavelength is 10.6 μm. The refractive indices of the silver halide and air at 10.6 μm are 2.1 and 1 respectively. The electrical vector of the light is perpendicular to the paper. (A meridional ray in the 1 mm diameter fibre propagates in the same way as for a planar waveguide.)

For the situation depicted in figure 5.5. the light from a CO_2 laser (10.6 μm) is launched at an angle of 45° to the waveguide axis. The ray is refracted at an angle of 20° and then follows the zigzag path with the incident angle at the boundary of 70°. The thickness of the waveguide is 1 mm. In this example, the electric vector is perpendicular to the paper, so the light propagates as the TE mode (q=1), and from equation 5.3, the power that propagates as the evanescent wave is 1.06% of the total power. If the light was launched as a TM mode, q

would be 3.84 (from equation 5.5) and the power propagating as the evanescent wave would be 0.17% of the total power. It is seen that the power in the evanescent field for the slab waveguide (and thick optical fibres), and hence the degree of interaction with the surrounding medium, is maximum when light is launched as a TE mode with the incident angle θ_1 as close to the critical angle as possible.

This calculation was carried out for an optical fibre (or a planar waveguide) with a surrounding lossless gas instead of cladding. When it is used as a sensor, the surrounding gas is not lossless, but the conclusion is the same: the degree of interaction with the surrounding medium is maximum when the light is launched as a narrow s-polarised (TE mode) beam with the incident angle θ_1 as close to the critical angle as possible.

5.2.4.2. Sensitivity of FEFA sensors

When light is transmitted through an FEFA sensor, the light measured at the output depends on the absorption of the evanescent field by the surrounding medium. When two-dimensional optics is applied, and the light follows a zigzag path inside the fibre, the relative transmittance function is given as (Messica *et al.*, 1994)

$$T(L,\lambda) \approx \exp(-\gamma L) + const \tag{5.6}$$

where L is the length of the sensing part of the fibre and γ is the effective fibre attenuation induced by the absorbing cladding or surrounding medium, which here is gaseous SF_6.

The sensitivity of an FEFA sensor depends on L and γ, while γ depends on several parameters: the radius and refractive index of the fibre core, the absorption coefficient and refractive index of the surrounding gas, and the nature of the light source. Again, two types of light source will be considered: a narrow laser beam reflecting back and forth at the waveguide boundary, and a wide-beam source which can be an incoherent source or a laser with a microscope objective. To distinguish these two cases, γ_N and γ_W will be used for the fibre attenuations for narrow-beam (N) and wide-beam (W) sources, respectively.

In the first case (narrow-beam source), the light beam is coupled as a high-order mode. The light can be coupled as a high-order mode (without exciting lower-order modes) by launching the beam along the fibre axis with the fibre in the form of a coil, or by launching the beam into the straight fibre at an angle. Rays in the fibre coil travel as whispering - gallery rays. A whispering - gallery ray is a ray in a curved fibre that reflects from the surface of the fibre as in figure 5.6. The bending method is more power efficient because less light is reflected from the input end of the fibre when the light is launched along the fibre axis. This can be important when a low-power laser diode is used.

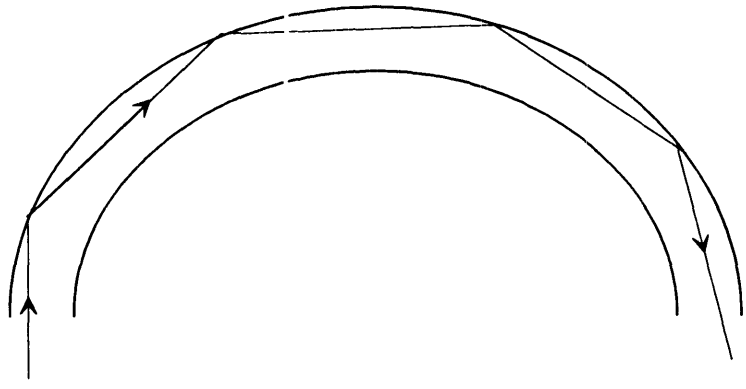

Figure 5.6. A whispering - gallery ray

Commercial optical fibres used for sensing at wavelengths above 2 μm have a diameter greater than 0.5 mm. This means that the V-number is much larger than 1 and the ray approach can be used to described the propagation of light within the fibre.

When this fibre is unclad and placed in a slightly absorbing medium ($n_i << n_{cl}$) and when a narrow laser beam is launched into the fibre, the attenuation of the light is given by (Schnitzer *et al.*, 1990)

$$\gamma_N L \approx \begin{cases} L\alpha(\Theta^2 + \delta^2) & 8\alpha_s L\Theta\delta < 3 \\ L\alpha(\Theta - \delta)^2 + \ln(8\alpha_s L\Theta\delta) & 8\alpha_s L\Theta\delta > 3 \end{cases} \tag{5.7}$$

where

n_i is defined in the complex refractive index $n = n_{cl} - in_i$,

$\Theta = \frac{\pi}{2} - \theta_1$ and θ_1 is the incident angle of the beam as defined in figure 5.5.,

δ is the beam divergence, and is much smaller than Θ;

$\alpha \equiv \frac{\alpha_s + \alpha_p}{2}$, where α_s and α_p are the effective absorption coefficients for

s (perpendicular) and p (parallel) polarisation with respect to the plane of incidence and

$\alpha_s \equiv \frac{a_{cl}C}{V}\tan^2\theta_c$; V is the V-number defined in appendix 3;

C is the concentration of the measurand that surrounds the fibre

and a_{cl} is the specific absorption of the cladding. In the literature a_{cl} can be found with different units: $cm^{-1}Pa^{-1}$ or cm^2mol^{-1}. An appropriate value for C has to be taken: in the first case it is the partial pressure in Pa, in the second it is the concentration in mol/cm^3.

$\theta_c = \arcsin\frac{n_{cl}}{n_{co}}$ is the critical angle and $\alpha_p \equiv \alpha_s(2 - \sin^2\theta_c)$.

For a wide-angle source, the attenuation is given by

$$\gamma_W L \approx \begin{cases} \frac{L\alpha\Theta^2}{2} & L\alpha\Theta^2 < 2 \\ \ln(L\alpha\Theta^2) & L\alpha\Theta^2 > 2 \end{cases} \qquad (5.8)$$

The condition $n_i << n_{cl}$ holds for all gases under normal conditions. For methane, at 1 atm and room temperature, $n_i = 2.2427 \times 10^{-4}$ at 3.392 μm (Stewart and

Culshaw, 1994). For dry air at 1 atm and room temperature, $n_i = 3.173 \times 10^{-11}$ at the wavelength of the P(16) CO_2 laser line (Wolfe and Zissis, 1978). Even for SF_6 at 10.548 μm (very close to the P(16) CO_2 laser line), 1 atm and 25 °C, n_i is 4.036×10^{-3} (Chapados and Birnbaum, 1988, from the graph in figure 4): 10.548 μm is one of two fundamental peaks in the absorption spectrum of SF_6 (see figure 7.1). Methane too has a strong absorption peak at 3.392 μm (Tai *et al.*, 1987). These values were calculated using the equation (Stewart and Culshaw, 1994)

$$n_i = \frac{aC\lambda}{4\pi} \tag{5.9}$$

and known values for the specific absorptions. In this equation, C is the concentration and a is the specific absorption.

From equations 5.7 and 5.8 it can be seen that γ for narrow-beam coupling depends linearly over a larger range than γ for wide-beam coupling, with the condition $\delta << \Theta$. For wide-beam coupling, γ becomes non-linear at $\alpha = \frac{2}{L\Theta^2}$ which is less than for narrow-angle coupling $\alpha_s = \frac{3}{8L\Theta\delta}$. In addition, the logarithm of response (and sensitivity) for wide-beam coupling is half of that for narrow-beam coupling.

In the CO_2 laser light absorption experiments described in chapter 7, the sensor operates in the linear regime under all conditions, because the quantity $8\alpha_s L\Theta\delta$ is much less than 3. Indeed, a value of 1.26×10^{-4} is obtained when the experimental parameters, listed below are substituted in

$$8\alpha_s L\Theta\delta \tag{5.10}$$

where

$\alpha_s = \frac{1}{V} a_{SF_6} C \tan^2\theta_c$

$V = 149765$,

$a_{SF_6} = 119$ m²/mol,

$C = 52.426$ mol/m³, which is the concentration at 130 kPa and 25 °C,

$L = 0.25$ m,

$\Theta = 19.677^{o} = 0.34343$ rad,
$\delta = 0.015$ rad, which is the divergence of the 1.5 mm diameter beam after passing through a biconvex lens of 4.25" (107.95 mm) focal length,

$$\theta_c = \arcsin\frac{1}{n_{co}} = \arcsin\frac{1}{2.1} = 0.495 \text{ rad}.$$

It may be concluded therefore that the sensor operates in the linear regime for all SF_6 pressures below 130 kPa at 25 °C, and this covers the experimental range of the present work.

5.2.5. Sensors based on the optomechanical effect

This type of optical fibre sensor is interferometric. A chemical reaction or mechanical process causes a change in the length of the fibre. For example, when palladium is coated on an optical fibre, the length changes when the Pd absorbs hydrogen (Butler, 1984). A change in length of the fibre can be measured very precisely if the fibre is in an interferometer arrangement.

5.2.6. Sensors based on plasmon surface resonance

These sensors use the glass-metal-substrate arrangement depicted in figure 5.7. When TM polarised light reflects from a thin metal film it may induce oscillation of charges on both surfaces of the metal layer. This occurs when the real part of the dielectric constant of the metal ε_m is smaller than the dielectric constant of the glass ε_g. The dielectric constant of the glass also has to be higher than the dielectric constant of the substrate ε_s (Richards *et al.*, 1993). The surface plasmons, which are surface electromagnetic waves (Dakin and Culshaw, 1988), propagate along the metal-substrate boundary with the surface plasmon propagation constant given by (Janata, 1989):

$$k_{sp} = \frac{\omega}{c}\frac{1}{\sqrt{\frac{1}{\varepsilon_m} + \frac{1}{\varepsilon_s}}} \tag{5.11}$$

where c is the velocity of light and ω is the angular frequency of the incident light. ε_m is frequency dependent and is given by

$$\varepsilon_m(\omega) = 1 - \left(\frac{\omega_p}{\omega}\right)^2 \tag{5.12}$$

where $\omega_p = 4\pi e^2 \frac{\rho}{m}$ is the plasma frequency for a free electron gas,

e is the electron charge,

ρ is the conduction electron number density and

m is the electron mass.

The component of light that travels parallel to the surface, on the glass side, has a propagation vector given by (Janata, 1989):

$$k_p = \sqrt{\varepsilon_g}\,\frac{\omega}{c}\sin\theta \tag{5.13}$$

where θ is the incident angle as shown in figure 5.7.

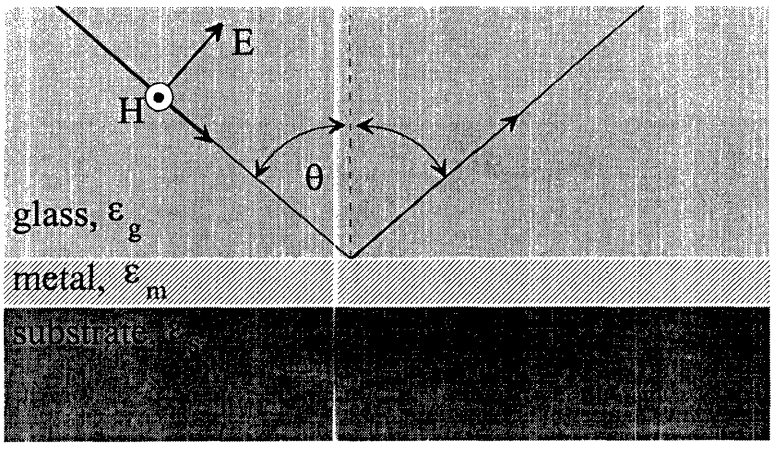

Figure 5.7. An arrangement for using plasmon surface resonance. The input light beam is p-polarised; that is, the electric field of the light wave lies in the plane defined by the incident and reflected beams.

A resonance occurs when k_p is equal to k_{sp}. For a wavelength that satisfies this condition there is strong attenuation of the incident light that can be detected through the attenuation of the reflected light (Swalen *et al.*, 1980). The intensity of the electric field of the

evanescent wave in the dielectric substrate is two orders of magnitude higher with the metal layer on the glass plate than without the metal layer (Culshaw and Dakin, 1989). The substrate can be a solid, liquid or gas material. Using plasmon surface resonance, refractive indices of gases, liquids and solid substances can be measured very precisely. The technique is sensitive enough to allow temperature measurement to be made from temperature-induced changes in refractive index (Chadwick and Gal, 1993). Optic fibre sensors based on plasmon surface resonance also can be designed. They can be made compact and structurally simple (Homola and Slavik, 1996), although they are somewhat less sensitive than their bulk optic counterparts (Kunz *et al.*, 1996).

5.3. Optical fibres for chemical sensing

Optical fibres have been developed mainly for telecommunications. They are usually silica-based or plastic-based with a small amount of dopant. Communications fibres have minimum light attenuation at 0.9 μm, 1 μm, 1.2 μm, 1.3 μm and 1.55 μm (Gowar, 1984). These fibres can be used for sensing but optimum performance is obtained with fibres designed specifically for sensing applications. These include birefringent fibres, D-fibres, fibres made of plastic mixed with luminescent material, fluoride fibres, silica fibres doped with germanium, silver halide fibres, polymer clad silica (PCS) fibres, chalcogenide fibres, fluoride fibres doped with heavy metals, hard plastic clad fibre, hollow fibres and nitrogen-doped silica fibres.

Here, some optical fibres designed specifically for chemical sensing will be described. High attenuation is not the problem for optical fibre sensors that it is for communications, and for example, silica fibres are used for methane detection at 3.392 μm (Tai *et al.* 1987) in spite of the high absorption of silica at this wavelength. However, low attenuation is sometimes an advantage even for sensing applications. For example, silver halide fibres have a transmission range of up to 16 μm and this makes them ideal for infrared spectroscopy (Schnitzer *et al.*, 1990). They can be used with or without cladding. Those

without cladding essentially use the surrounding air as cladding. Chalcogenide optical fibres have better mechanical properties (Busse *et al.*, 1996) but their transmission range extends only to 11 μm which is still good enough to allow them to be used for infrared spectroscopy. Silver halide optical fibres will be described in more detail in the experimental section 5.3.2 on SF_6 sensing.

Silica fibres can be used for evanescent-field absorption measurements as some diatomic molecules have absorption peaks in the visible spectrum: for example, Cl_2 has an absorption peak at 530 nm (Safaai-Jazi and Petersen, 1994). Polymer-clad silica fibres and hard-plastic clad fibres are suitable for this application. Polymer-clad silica fibres have a silica core, and cladding made of silicone. This makes the cladding easy to remove and the core can be readily exposed to the surrounding medium. The cladding of hard plastic-clad fibres is made of hard polymer that can be removed easily with chemicals without etching the core.

Optical fibre sensors which rely on phase or polarisation modulation use single-mode fibres and polarised light. However, conventional single-mode fibres with circular cross-section permit the propagation of two nearly degenerate modes with orthogonal polarisation, and coupling between these modes results in the input polarisation not being retained as light propagates through the fibre. This problem is overcome by using one of several types of optical fibre which permit light to pass through whilst retaining its state of polarisation. These polarisation- maintaining fibres can be classified into two general groups, which are termed high-birefringence (Hi-Bi) and low birefringence (Low-Bi) (Dakin and Culshaw, 1988). In one type of Hi-Bi fibre, the circular symmetry of the core is removed so that the two modes have significantly different propagation constants: this hinders coupling between modes so that light polarised along a principal axis of the fibre maintains its polarisation. Fibres of this type include elliptical-core, bow-tie and PANDA. Another type of Hi-Bi fibre allows only one polarisation mode to propagate by imposing a cut-off condition on the other mode. Bow-tie and PANDA fibres can be designed in this way. On the other hand, the residual linear birefringence within a conventional fibre can be substantially reduced by introducing a high degree of circular birefringence. Methods of doing this, and thus producing

Low-Bi fibres, include twisting a conventional single-mode fibre after manufacture, and rotating the glass preform during the fibre drawing process to produce spun fibre.

Polarisation-maintaining optical fibres do not find many applications in chemical sensing. However, when a fibre is used to deliver light to a sensor based on surface plasmon resonance, polarisation is important, and polarisation-maintaining fibres are used for such devices (Richards *et al.*, 1993).

5.3.1. Polymer-clad silica fibres

Some polymer-clad silica (PCS) fibres can be stripped of their polymer cladding by mechanical means, while others require chemical stripping with, for example, Lumer optical fibre stripper "S".

In the sulphur deposition experiment (chapter 6), a mechanically strippable fibre, made by Ceram Optec, was used. Its commercial name is PCS 600N PUV. This version has enhanced UV transmission and a nylon jacket. The Ceram Optec fibre has a high numerical aperture: 0.4 for 2 m length and 0.3 for lengths longer than 40 m. The core is made of pure fused silica. The diameter is 600 μm, and the thickness of each of the cladding and jacket is 50 μm. The maximum bend radius is 100 times the core radius for short-term bending and for long-term bending, 600 times the core radius.

5.3.2. Silver halide fibre

For the experiment described in chapter 7, unclad silver halide optical fibre was chosen because it is readily available. The properties of the silver halide optical fibre type MIR 1000, supplied by Ceram Optec, are listed below:

- Non hygroscopic material		- Attenuation @ 10.6 μm	less than 0.5 dB/m
- Insoluble in water (Eyal *et al.*, 1994)		- Effective NA	0.5
- Non-toxic material		- Fibre material	$AgBr_xCl_{1-x}$
- Non brittle and flexible		- Density	6390 kg/m^3
- Fibre diameter	1 mm	- Melting point	412 °C
- Transmission range	5 to 16 μm	- Tensile strength	100 MPa
- Damage threshold	10 kW/cm^2	- Minimum bend radius	10 mm for 0.7 mm core
- Refractive index	2.1		

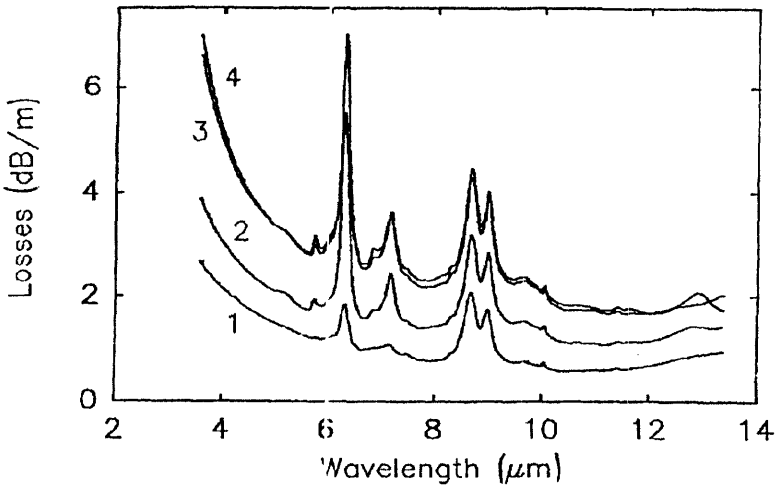

Figure 5.8. Total losses in $AgBr_{0.75}Cl_{0.25}$ fibre measured immediately after production (1), after 5 months (2), after 9 months (3) and after 12 months (4). (Grigorjeva *et al.*, 1996).

Silver halide fibres are made by extrusion from a monocrystal of $AgBr_xCl_{1-x}$ but the extruded fibre has a polycrystalline structure. The size of the crystal grains in the fibre increases with time, and attenuation increases due to this ageing effect as shown in figure 5.8. Ultraviolet and blue light cause the formation of colloidal silver centres in silver halide fibres. This changes the colour of the fibre from yellow to dark blue, and increases fibre losses at all wavelengths. While the ageing process is not so important when these fibres are used for CO_2 laser beam delivery, it is very important when the fibres are used for sensing. This increase in attenuation must be taken into account in sensor design. The increase depends on many factors, but mainly on the manufacturing procedure. To avoid any error in measurement due to the ageing process there should be a reference fibre arm in the measurement system. The reference fibre can be linked with the measuring fibre through a Y coupler, and it is relatively easy to make a Y coupler with silver halide fibres (Eyal *et al.*, 1994). Another possibility is to send two beams at different wavelengths into the same fibre, one at the absorption peak and another one far from that. Changing the intensity of the non-absorptive beam allows a correction factor to be calculated.